Supporting Information for "Retreat of the Antarctic Ice Sheet during the Last Interglaciation and implications for future change"

N. R. Golledge[1], P. U. Clark[2,3], F. He[4], A. Dutton[5], C. S. M. Turney[6,7,8], C. J. Fogwill[6,9,10], T. R. Naish[1], R. H. Levy[1,11], R. M. Mckay[1], D. P. Lowry[11], N. A. N. Bertler[1,11], G. B. Dunbar[1], A. E. Carlson[12]

[1]Antarctic Research Centre, Victoria University of Wellington, Wellington 6140, New Zealand
[2]College of Earth, Ocean, and Atmospheric Sciences, Oregon State University, Corvallis, OR, USA
[3]School of Geography and Environmental Sciences, University of Ulster, Coleraine, UK
[4]Center for Climatic Research, Nelson Institute for Environmental Studies, University of Wisconsin-Madison, Madison, WI, USA
[5]Department of Geoscience, University of Wisconsin-Madison, Madison, WI, USA
[6]Earth and Sustainability Science Research Centre, School of Biological, Earth and Environmental Sciences, University of New South Wales, Kensington NSW 2033, Australia
[7]Australian Research Council Centre of Excellence in Australian Biodiversity and Heritage, School of Biological, Earth and Environmental Sciences, University of New South Wales, Kensington NSW 2033, Australia
[8]Chronos 14 Carbon-Cycle Facility, University of New South Wales, Sydney NSW 2052, Australia
[9]School of Geography, Geology and the Environment, Keele University, Staffordshire ST5 5BG, UK
[10]School of Water, Energy and the Environment, Cranfield University, College Road, Cranfield, MK43 0AL, UK
[11]GNS Science, Avalon, Lower Hutt 5011, New Zealand
[12]Oregon Glaciers Institute, Corvallis OR 97330, USA

Contents of this file

Uncertainties associated with glacial isostatic adjustment

One of the key advances we present in this paper, compared to our previous simulations for the LIG (Clark et al., 2020), is that our stiffer mantle parameterisation yields maximum ice loss earlier in the interglacial period, reaching a peak at 126 ka followed by subsequent ice sheet regrowth and sea level fall. This contrasts markedly with the former parameterisation that instead produced a long sustained peak sea-level contribution from 124 ka (Clark et al., 2020). The cause of these changes in timing and magnitude of mass loss is the mantle viscosity parameterisation, which in the new simulations is increased to 1.3×10^{20} Pa s, from the previous 1.0×10^{19}. Whilst this change allows a much closer fit to probabilistic interpretations of the Antarctic contribution to LIG GMSL (Kopp et al., 2009), we note that Kopp et al. (2009) caution the use of their ice volume projections on the basis that in their assessment they use a Gaussian distribution to represent a non-Gaussian prior. Furthermore we acknowledge that our isostatic parameterisation remains an area of considerable uncertainty and so provide further discussion of this part of our methodology here.

In the version of PISM that we employ here (v.0.7.1) we are limited to a 1-dimensional isostatic adjustment scheme that uses a single upper mantle viscosity and a single lithospheric rigidity value for the entire domain. It is therefore not possible for us to accomodate spatial heterogeneity in the isostatic model. This is common for most ice sheet models, and is directly comparable (in terms of simplification of approach) to previous LIG AIS simulations (Goelzer et al., 2016; DeConto & Pollard, 2016). Although those two studies employ different ice sheet models, both use the same radially-symmetric 1-dimensional isostatic scheme, based on Huybrechts and De Wolde (1999). According to Huybrechts (2002, p.205), this scheme yields bedrock deformation results beneath the Antarctic continent that are, '...close to those from a full visco-elastic treatment with mantle viscosities in the range 0.5-1.0 $\times 10^{21}$ Pa s'. Our value of 1.3×10^{20} Pa s represents a mantle rheology that is therefore 4 to 8 times less viscous than those studies, resulting in faster rebound in areas where ice is lost. In order to provide a broader context for these uncertain values, we collated inferences of upper mantle viscosity values from published studies (Table S2).

From Table S2 it can be seen that relatively weak Antarctic mantle exists beneath the Antarctic Peninsula, where values in the range 1×10^{18} to 1×10^{20} Pa s are common, and beneath the Amundsen Sea Embayment of West Antarctica, where inferences are mostly in the range 1×10^{17} to 1×10^{19} Pa s. Other sectors of West Antarctica, such as the southern Weddell Sea and the Siple Coast, are underlain by stronger mantle with viscosities typically in the range 1×10^{20} to 1×10^{21} Pa s. It is clear that the types of radially-symmetric isostatic models that our new experiments and other LIG studies have used do not fully capture the heterogeneity of asthenospheric properties inferred from geophysical observations and modelling studies. The primary impact of our use of a mantle viscosity that is stronger than inferred for some parts of West Antarctica would be the delayed rebound of bedrock following ice retreat. Figures S3 & S4 illustrate how sensitive our model is to this aspect of model parameterisation. However, we have employed what we believe to be a unique and rigorous tuning and validation procedure, in which we constrain our model parameterisation to values that allow the well-mapped Last Glacial Maximum (LGM) and present-day (PD) grounding line positions to be closely matched. If our isostatic scheme were too far from realistic values, we would either accelerate (if the mantle were too stiff) or delay (if the mantle were too fluid) retreat of the LGM ice sheet and we would not be able to reproduce PD grounding lines as well as we do (Fig. S4). To our knowledge, no LIG studies other than the present manuscript and our previous work (Clark et al., 2020) employ such an independent validation. On this basis we are confident that our model formulation is not only robust but is also closer to empirically-derived mantle rheologies than some previous studies. Nonetheless, we acknowledge that our solution in non-unique, and that further investigation would be valuable.

Uncertainty related to ocean temperature forcing

A further source of uncertainty in our simulations arises from the way in which we supply ocean thermal forcing to our modelled ice sheet. All LIG Antarctic Ice Sheet simulations have approached this problem differently. Goelzer et al. (2016) used a fully coupled ice-sheet–atmosphere–ocean model to simulate global climate and both the Greenland and Antarctic ice sheets in a consistent framework. They did not need to apply additional oceanic heat flux to drive West Antarctic Ice Sheet retreat. The spatial pattern of the LIG circum-Antarctic ocean temperature anomaly simulated by their model is not shown, however. DeConto and Pollard (2016) did not use model-based LIG ocean temperatures but instead used a present-day temperature map from the World Ocean Atlas (Levitus et al., 2012) to which they added spatially-uniform thermal anomalies (+3 to +4°C) un-

til ice sheet retreat was triggered. Sutter, Gierz, Grosfeld, Thoma, and Lohmann (2016) used a fully-coupled atmosphere-ocean general circulation model (AOGCM) to simulate LIG ocean temperature anomalies but also added spatially-uniform thermal forcing of +1 to +3°C in order to investigate the temperature threshold for collapse of West Antarctica. In our study we use a fully-coupled AOGCM to derive an oceanic forcing that is applied as an uncoupled transient forcing to our ice sheet model. We do not impose additional oceanic heat flux, but note that the ice–ocean feedback process (Menviel et al., 2010; Golledge et al., 2014) would have most likely increased subsurface warming and enhanced ice shelf basal melting. The spatial pattern of warming at the time of peak warmth (128.5 ka BP) at depths below the mixed layer in our CCSM3 simulations is shown in Figure S5. We observe strong warming offshore Dronning Maud Land (30°W to 30°E), strong cooling offshore Wilkes Land (80°E to 150°E), cooling in the Ross Sea embayment (170°E to 160°W), warming in the Amundsen Sea embayment and along the western Antarctic Peninsula (130°W to 60°W), and cooling in the Weddell Sea (60°W to 30°W). This distribution is qualitatively similar to results from Sutter et al. (2016) with the exceptions that they observe less cooling in the Ross and Weddell seas compared to our model, and less warming in the Amundsen Sea. Although there are no high-latitude ocean temperature proxies available to constrain circum-Antarctic temperatures south of approximately 50°S, we note that our simulated pattern of warming captures the same basic pattern as indicated for the current century in the multi-model mean of Climate Model Intercomparison Project Phase 5 (CMIP5) simulations, under Representative Concentration Pathway 8.5 (Naughten et al., 2018).

CCSM3 has been used to simulate a reasonable climate evolution of the deglacial surface temperature over Greenland, the surface ocean of the Southern Hemisphere, and over Antarctica (He et al., 2013; Buizert et al., 2014) as well as subsurface ocean temperature during Heinrich events in the North Atlantic (Marcott et al., 2011). We therefore have confidence in our simulated ocean thermal forcing prescription, but acknowledge that a different pattern of warming could produce a different pattern of ice retreat, with potential impacts on the AIS contribution to GMSL. However, our spatial pattern of mass loss is consistent with geologically-based inferences of ice sheet collapse in the Amundsen Sea sector (Carlson et al., 2021), with glaciological evidence of inland thinning in the southern Weddell Sea sector (Turney et al., 2020), and with geological signatures of enhanced ice sheet discharge offshore the Wilkes Subglacial Basin (Wilson et al., 2018). To-date, no conclusive records exist with which to either prove or disprove loss of ice from the Ross or Weddell Sea embayments during the LIG.

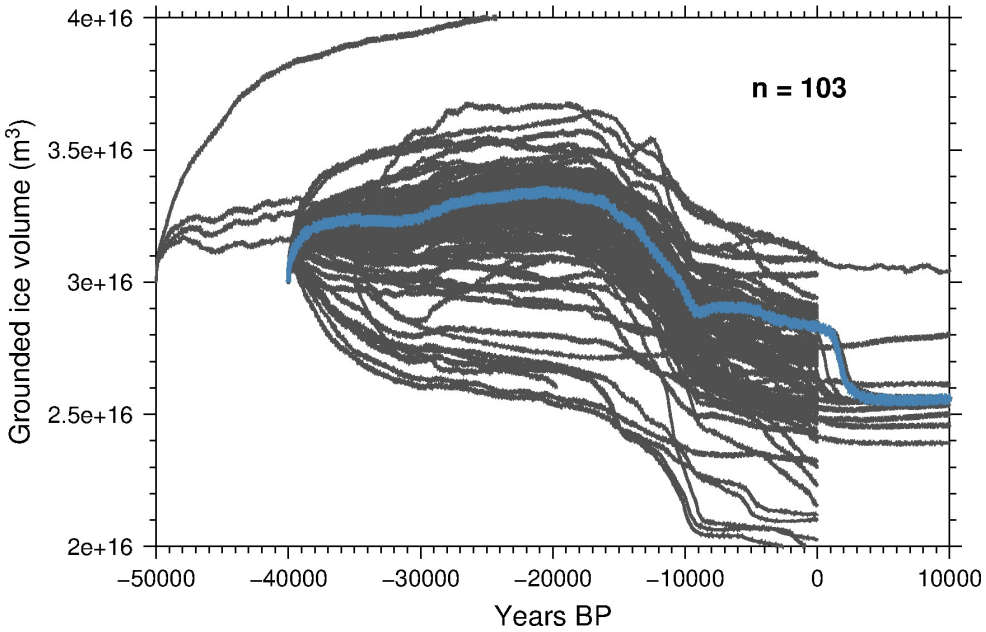

Figure S1. Evolution of grounded ice volume for the T1 experiment for 103 simulations that explore different parameterisations for flow enhancement factors, sliding exponents, substrate rheology, and grounding line schemes. Blue line shows the reference configuration (1.3e20 Pa s).

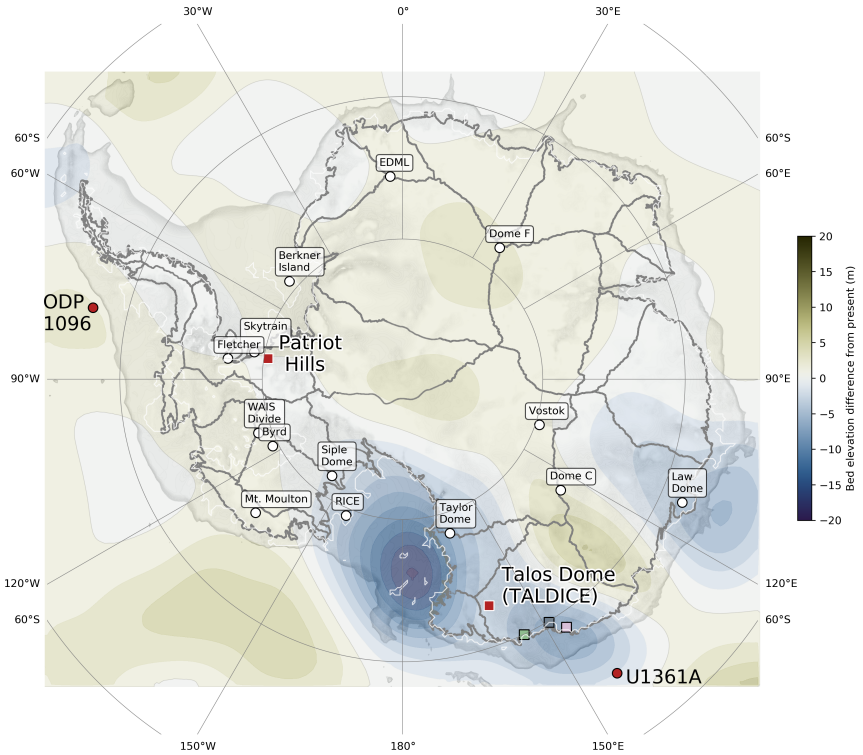

Figure S2. Bed elevation difference at 130 ka BP compared to present, based on linear interpolation of a Pliocene reconstruction of dynamic topography (Austermann et al., 2015). Changes in locations where the present-day ice sheet grounding line occurs are typically in the range -10 to +10 m. Grey lines show present-day boundaries of grounded ice catchments (Zwally et al., 2012). Patriot Hills blue ice area, Talos Dome ice core site, ODP1096 and U1361A marine sediment core locations and the three sites (coloured boxes) investigated in Figure 4 also shown. Labeled white squares identify ice core locations for which predictions of ice sheet change are presented in Figure S5.

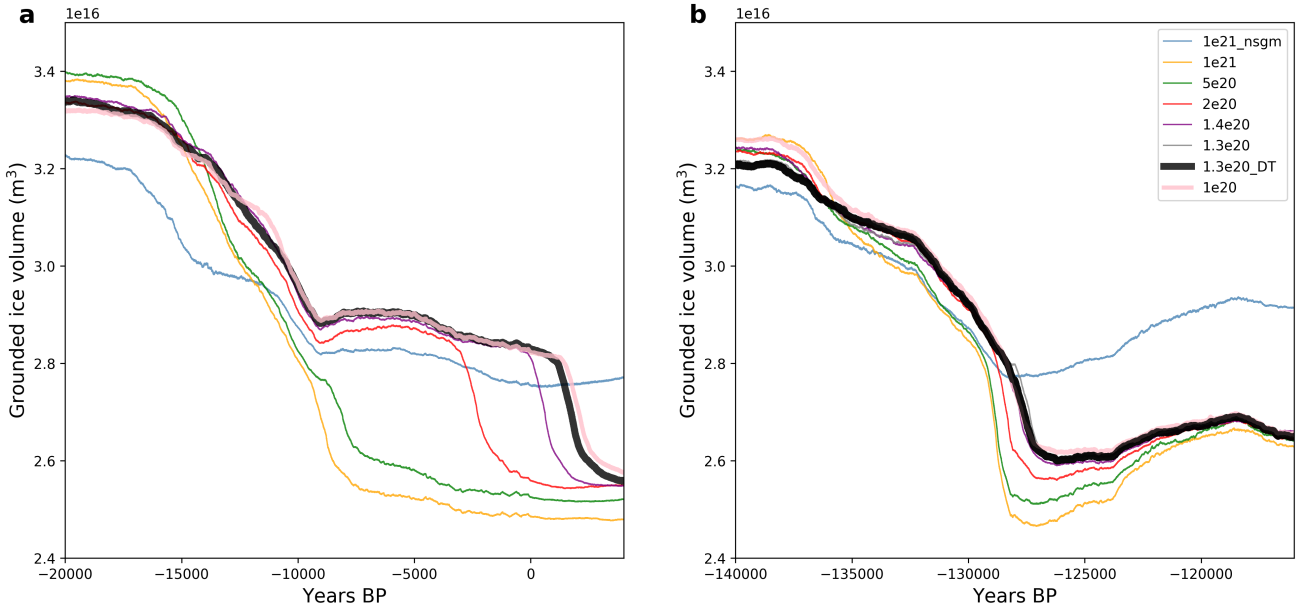

Figure S3. Impact of mantle viscosity variations on ice sheet evolution under T1 and T2 forcings. a) Timeseries of grounded ice volume for the last deglaciation (T1), used as a tuning experiment. Black line illustrates the reference experiment used as the basis for interpretations presented in this paper, pink line shows value used in previous simulations (Clark et al., 2020). Stiffer mantle viscosities lead to collapse of WAIS before simulated present-day ('Year 0') is reached. b) The same experiments as in a) but for the T2 climatology. Collapse of WAIS takes place earliest for stiffer mantle parameterisations, with only a very narrow range able to reproduce present-day grounding line extent as well as a multi-metre LIG contribution to sea level. Blue line in both panels illustrates a simulation in which the sub-grid grounding line scheme is turned off, effectively preventing the ice sheet from advancing or retreating adequately.

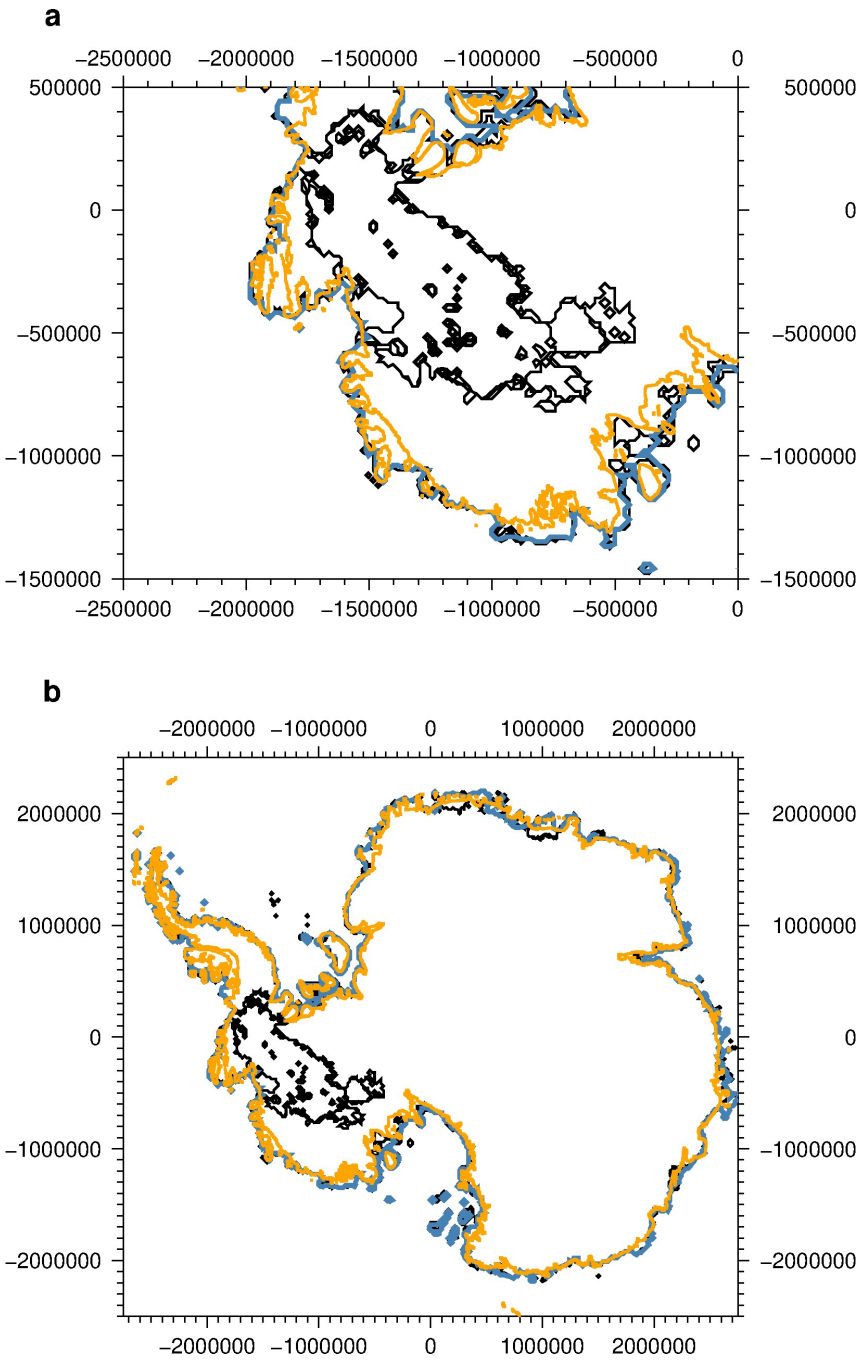

Figure S4. Impact of mantle viscosity variations on modelled present-day grounding line positions for a) West Antarctica, and b) the whole continent. In blue, the grounding line as represented by the reference configuration (1.3e20 Pa s) for the T1 experiment. Mantle viscosities greater than this lead to WAIS grounding line retreat to positions (black lines) further inland than the present-day observations (gold line) show.

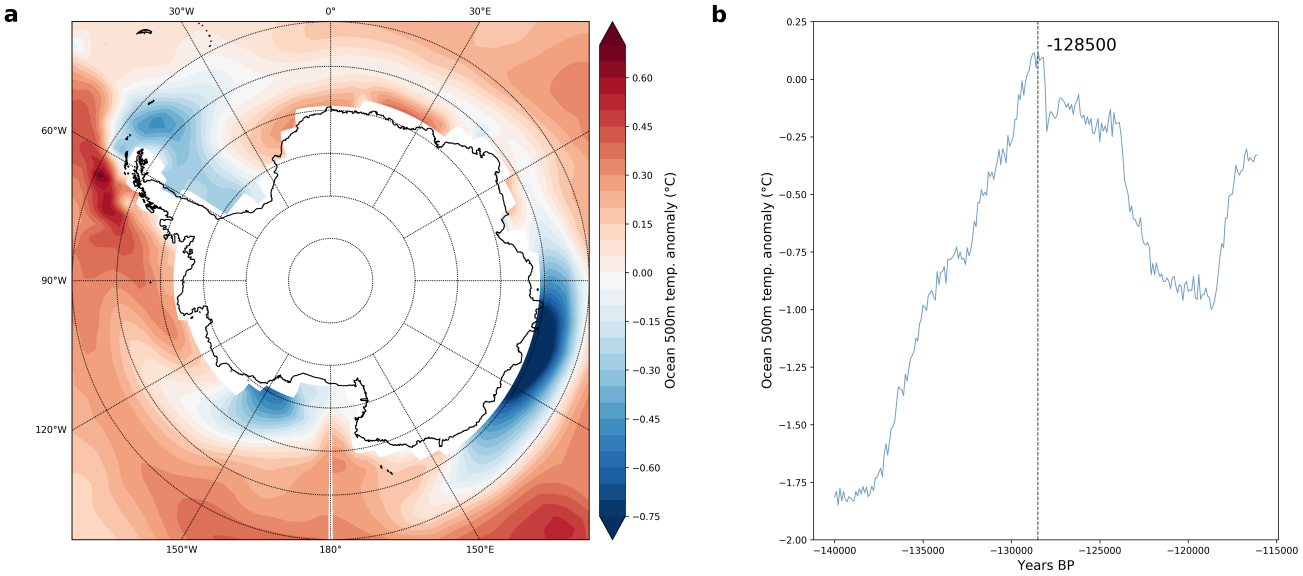

Figure S5. a) Ocean temperature (as anomalies from modelled present) simulated by CCSM3 for 500 m depth at the time of peak warmth (128.5 ka BP). Warming close to the Antarctic coast is evident along the western Antarctic Peninsula and into the Amundsen Sea Embayment, but cooler-than-present conditions prevail in the Weddell Sea and Ross Sea embayments. b) Zonally-averaged ocean temperature anomalies at 500 m depth from CCSM3. Vertical line shows peak warmth timeslice illustrated in a).

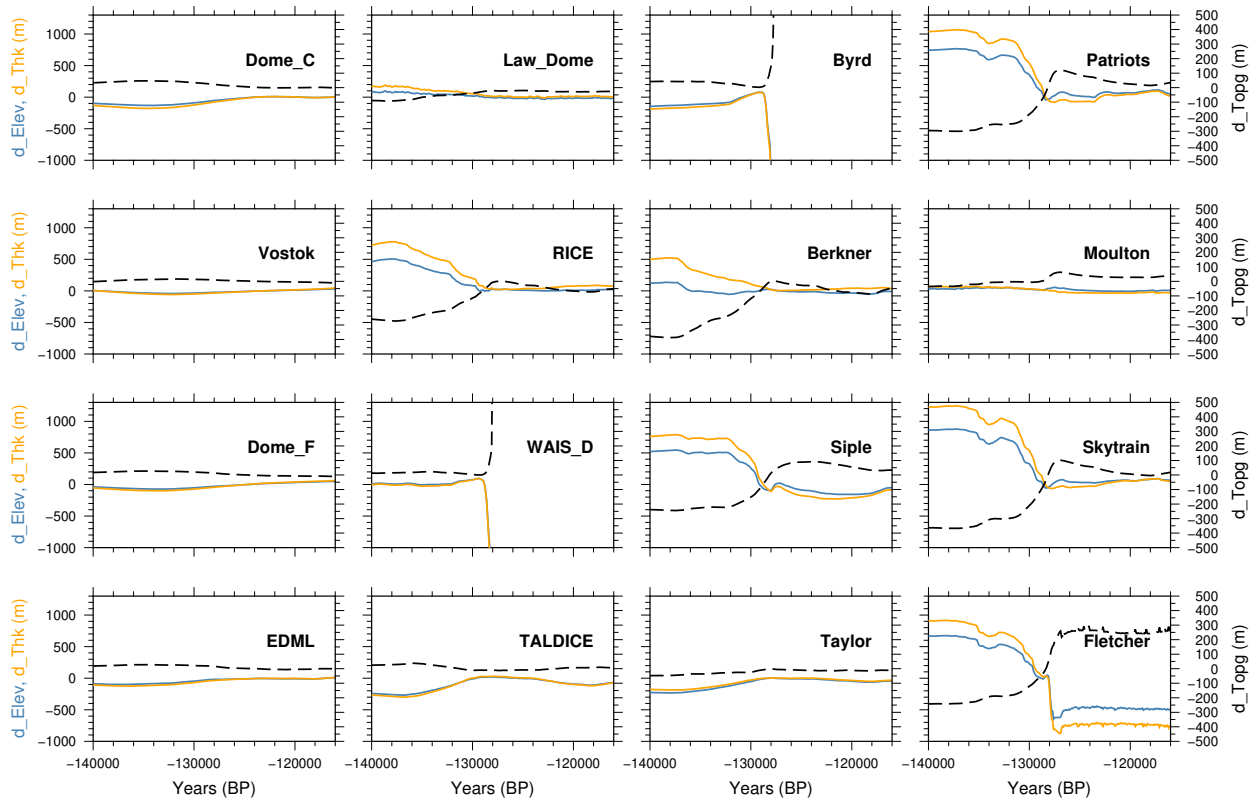

Figure S6. Changes in modelled ice thickness (gold), surface elevation (blue), and bed elevation (black) at each of the ice core sites shown in Figure 1c, shown as deviations from modelled present-day values at each site. Note the different scaling for the bed elevation changes (righthand axes) compared to that used for ice thickness and surface elevation (lefthand axes).

Table S1. Parameters used in the reference simulations for T1 and T2 experiments.

Parameter	Value	Units
PISM version	0.7.1	–
Domain x	289	cells
Domain y	249	cells
Vertical ice layers	121	–
Vertical bedrock layers	20	–
Computational box height	6000	m
z spacing (ice)	quadratic	–
z spacing (bedrock)	equal	–
shallow-ice approximation enhancement	1.75	–
shallow-shelf approximation enhancement	1.0	–
pseudo plastic q	0.25	–
eigen calving K	1e18	–
Thickness calving threshold	180	m
Grounding line scheme	subgrid	–
Till porewater overburden fraction	0.05	–
Atmospheric lapse rate	8	°C

Table S2. Inferences of upper mantle viscosity values for a range of locations and depths in West Antarctica. Where depth is unspecified, the value is assumed to apply to the full thickness of the upper mantle (approximately 660 km).

Study	Location	Depth	Viscosity
Simms et al., (2012)	South Shetland Islands	–	$1\text{x}10^{18}$ Pa s
Nield et al. (2014)	northern Antarctic Peninsula	–	$\leq 1\text{x}10^{18}$ Pa s
Samrat et al. (2020)	northern Antarctic Peninsula	above 400 km	$0.3 - 3\text{x}10^{18}$ Pa s
Samrat et al. (2020)	northern Antarctic Peninsula	below 400 km	$4\text{x}10^{20}$ Pa s
Ivins et al. (2011)	northern Antarctic Peninsula,	–	$4–7\text{x}10^{19}$ Pa s
Zhao et al. (2017)	central Antarctic Peninsula	–	$> 2\text{x}10^{19}$ Pa s
Wolstencroft et al. (2015)	southern Antarctic Peninsula	–	$1 - 3\text{x}10^{20}$ Pa s
Bradley et al., (2015)	southern Weddell Sea	–	$1\text{x}10^{21}$ Pa s
Barletta et al. (2018)	Amundsen Sea Embayment	65-200 km	$4\text{x}10^{18}$ Pa s
Barletta et al. (2018)	Amundsen Sea Embayment	200-400 km,	$1.6\text{x}10^{19}$ Pa s
Barletta et al. (2018)	Amundsen Sea Embayment	400-660 km	$2.5\text{x}10^{19}$ Pa s
Powell et al., (2020)	Amundsen Sea Embayment	–	$1\text{x}10^{17} - 1\text{x}10^{19}$ Pa s
Nield et al., (2016)	central Siple Coast	–	$\geq 1\text{x}10^{20}$ Pa s

References

Austermann, J., Pollard, D., Mitrovica, J. X., Moucha, R., Forte, A. M., DeConto, R. M., ... Raymo, M. E. (2015). The impact of dynamic topography change on Antarctic ice sheet stability during the mid-Pliocene warm period. *Geology*, *43*(10), 927–930.

Barletta, V. R., Bevis, M., Smith, B. E., Wilson, T., Brown, A., Bordoni, A., ... others (2018). Observed rapid bedrock uplift in Amundsen Sea Embayment promotes ice-sheet stability. *Science*, *360*(6395), 1335–1339.

Bradley, S. L., Hindmarsh, R. C. A., Whitehouse, P. L., Bentley, M. J., & King, M. A. (2015). Low post-glacial rebound rates in the weddell sea due to late holocene ice-sheet readvance. *Earth and Planetary Science Letters*, *413*, 79–89.

Buizert, C., Gkinis, V., Severinghaus, J. P., He, F., Lecavalier, B. S., Kindler, P., ... others (2014). Greenland temperature response to climate forcing during the last deglaciation. *Science*, *345*(6201), 1177–1180.

Carlson, A. E., Beard, B. L., Hatfield, R. G., & Laffin, M. (2021). Absence of West Antarctic-sourced silt at ODP Site 1096 in the Bellingshausen Sea during the last interglaciation: Support for West Antarctic ice-sheet deglaciation. *Quaternary Science Reviews*, *261*, 106939.

Clark, P. U., He, F., Golledge, N. R., Mitrovica, J. X., Dutton, A., Hoffman, J. S., & Dendy, S. (2020). Oceanic forcing of penultimate deglacial and last interglacial sea-level rise. *Nature*, *577*, 660-664.

DeConto, R., & Pollard, D. (2016). Contribution of Antarctica to past and future sea-level rise. *Nature*, *531*, 591-597.

Goelzer, H., Huybrechts, P., Loutre, M.-F., & Fichefet, T. (2016). Last Interglacial climate and sea-level evolution from a coupled ice sheet–climate model. *Climate of the Past*, *12*(12), 2195–2213.

Golledge, N., Menviel, L., Carter, L., Fogwill, C., England, M., Cortese, G., & Levy, R. (2014). Antarctic contribution to meltwater pulse 1A from reduced Southern Ocean overturning. *Nature Communications*, *(5)*, 1-10. doi: doi:10.1038/ncomms6107

He, F., Shakun, J. D., Clark, P. U., Carlson, A. E., Liu, Z., Otto-Bliesner, B. L., & Kutzbach, J. E. (2013). Northern Hemisphere forcing of Southern Hemisphere climate during the last deglaciation. *Nature*, *494*(7435), 81–85.

Huybrechts, P. (2002). Sea-level changes at the LGM from ice-dynamic reconstructions of the Greenland and Antarctic ice sheets during the glacial cycles. *Quaternary Science Reviews*, *21*(1-3), 203–231.

Huybrechts, P., & De Wolde, J. (1999). The dynamic response of the greenland and antarctic ice sheets to multiple-century climatic warming. *Journal of Climate*, *12*(8 PART 1), 2169–2188.

Ivins, E. R., Watkins, M. M., Yuan, D.-N., Dietrich, R., Casassa, G., & Rülke, A. (2011). On-land ice loss and glacial isostatic adjustment at the Drake Passage: 2003–2009. *Journal of Geophysical Research: Solid Earth*, *116*(B2).

Kopp, R. E., Simons, F. J., Mitrovica, J. X., Maloof, A. C., & Oppenheimer, M. (2009, December). Probabilistic assessment of sea level during the last interglacial stage. *Nature*, *462*(7275), 863–867. doi: 10.1038/nature08686

Levitus, S., Antonov, J. I., Boyer, T. P., Baranova, O. K., Garcia, H. E., Locarnini, R. A., ... others (2012). World ocean heat content and thermosteric sea level change (0–2000 m), 1955–2010. *Geophysical Research Letters*, *39*(10).

Marcott, S. A., Clark, P. U., Padman, L., Klinkhammer, G. P., Springer, S. R., Liu, Z., ... Schmittner, A. (2011). Ice-shelf collapse from subsurface warming as a trigger for Heinrich events. *Proceedings of the National Academy of Sciences*, *108*, 13415-13419.

Menviel, L., Timmermann, A., Timm, O. E., & Mouchet, A. (2010). Climate and biogeochemical response to a rapid melting of the West Antarctic Ice Sheet during interglacials and implications for future climate. *Paleoceanography*, *25*.

Naughten, K. A., Meisssner, K. J., Galton-Fenzi, B. K., England, M. H., Timmermann, R., & Hellmer, H. H. (2018). Future Projections of Antarctic Ice Shelf Melting Based on CMIP5 Scenarios. *Journal of Climate*, *31*, 5243-5261.

Nield, G. A., Barletta, V. R., Bordoni, A., King, M. A., Whitehouse, P. L., Clarke, P. J., ... Berthier, E. (2014). Rapid bedrock uplift in the Antarctic Peninsula explained by viscoelastic response to recent ice unloading. *Earth and Planetary Science Letters*, *397*, 32–41.

Nield, G. A., Whitehouse, P. L., King, M. A., & Clarke, P. J. (2016). Glacial isostatic adjustment in response to changing Late Holocene behaviour of ice streams on the Siple Coast, West Antarctica. *Geophysical Supplements to the Monthly Notices of the Royal Astronomical Society*, *205*(1), 1–21.

Powell, E., Gomez, N., Hay, C., Latychev, K., & Mitrovica, J. (2020). Viscous effects in the solid Earth response to modern Antarctic ice mass flux: Implications for geodetic studies of WAIS stability in a warming world.

Journal of Climate, *33*(2), 443–459.

Samrat, N. H., King, M. A., Watson, C., Hooper, A., Chen, X., Barletta, V. R., & Bordoni, A. (2020). Reduced ice mass loss and three-dimensional viscoelastic deformation in northern Antarctic Peninsula inferred from GPS. *Geophysical Journal International*, *222*(2), 1013–1022.

Simms, A. R., Ivins, E. R., DeWitt, R., Kouremenos, P., & Simkins, L. M. (2012). Timing of the most recent Neoglacial advance and retreat in the South Shetland Islands, Antarctic Peninsula: insights from raised beaches and Holocene uplift rates. *Quaternary Science Reviews*, *47*, 41–55.

Sutter, J., Gierz, P., Grosfeld, K., Thoma, M., & Lohmann, G. (2016). Ocean temperature thresholds for last interglacial West Antarctic ice sheet collapse. *Geophysical Research Letters*, *43*(6), 2675–2682.

Turney, C., Jones, R., McKay, N., Van Sebille, E., Thomas, Z., Hillenbrand, C.-D., & Fogwill, C. (2020). A global mean sea surface temperature dataset for the Last Interglacial (129–116 ka) and contribution of thermal expansion to sea level change. *Earth System Science Data*, *12*(4), 3341–3356.

Wilson, D. J., Bertram, R. A., Needham, E. F., van de Flierdt, T., Welsh, K. J., McKay, R. M., ... Escutia, C. (2018). Ice loss from the East Antarctic Ice Sheet during late Pleistocene interglacials. *Nature*, *561*(7723), 383–386.

Wolstencroft, M., King, M. A., Whitehouse, P. L., Bentley, M. J., Nield, G. A., King, E. C., ... others (2015). Uplift rates from a new high-density GPS network in Palmer Land indicate significant late Holocene ice loss in the southwestern Weddell Sea. *Geophysical Journal International*, *203*(1), 737–754.

Zhao, C., King, M. A., Watson, C. S., Barletta, V. R., Bordoni, A., Dell, M., & Whitehouse, P. L. (2017). Rapid ice unloading in the Fleming Glacier region, southern Antarctic Peninsula, and its effect on bedrock uplift rates. *Earth and Planetary Science Letters*, *473*, 164–176.

Zwally, H. J., Giovinetto, M. B., Beckley, M. A., & Saba, J. L. (2012). Antarctic and Greenland Drainage Systems. *GSFC Cryospheric Sciences Laboratory*, http://icesat4.gsfc.nasa.gov/cryo_data/ant_grn_drainage_systems.php.